Supplementary Information

A Disulfide–Fe^{3+} Crosslinking Strategy for Tough Hydrogel Networks with Complete Photo- and Biochemical Degradability

Young Bin Yoon,[a] Nakhyun Kim,[a] Hoeyun Jung,[a] Yoonha Ko,[cde] Chan Kang,[a] Jooyeun Chong,[f] Jiheong Kang,[f] Dongmin Kang[cde] and Jae-Byum Chang*[abe]

a. *Department of Materials Science and Engineering, Korea Advanced Institute of Science and Technology (KAIST), Daejeon 34141, Republic of Korea*

b. *Department of Biological Sciences, Korea Advanced Institute of Science and Technology (KAIST), Daejeon 34141, Republic of Korea*

c. *Department of Life Science, Ewha Womans University, Seoul 03760, Republic of Korea*

d. *Fluorescence Core Imaging Center, Ewha Womans University, Seoul 03760, Republic of Korea*

e. *Bioimaging Data Curation Center, Seoul 03760, Republic of Korea*

f. *Department of Chemistry, Seoul National University, Seoul 08826, Republic of Korea*

* Corresponding authors.

E-mail address: jbchang03@kaist.ac.kr

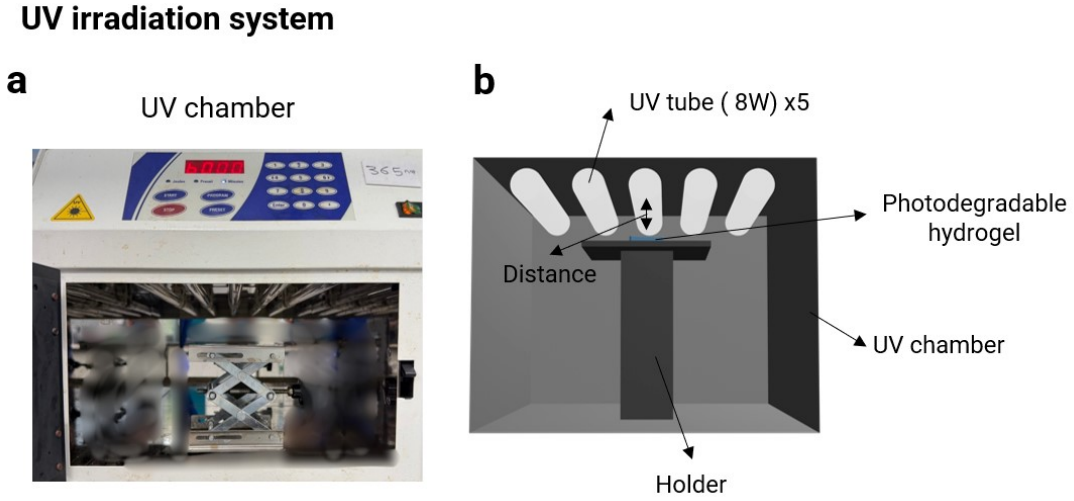

Figure S1. Schematic illustration of the UV irradiation setup: (a) photographs of the UV chamber and (b) a schematic diagram of the experimental configuration inside the chamber. The sample holder is height-adjustable, and the standard lamp–sample distance used in this study was 3 mm unless otherwise noted.

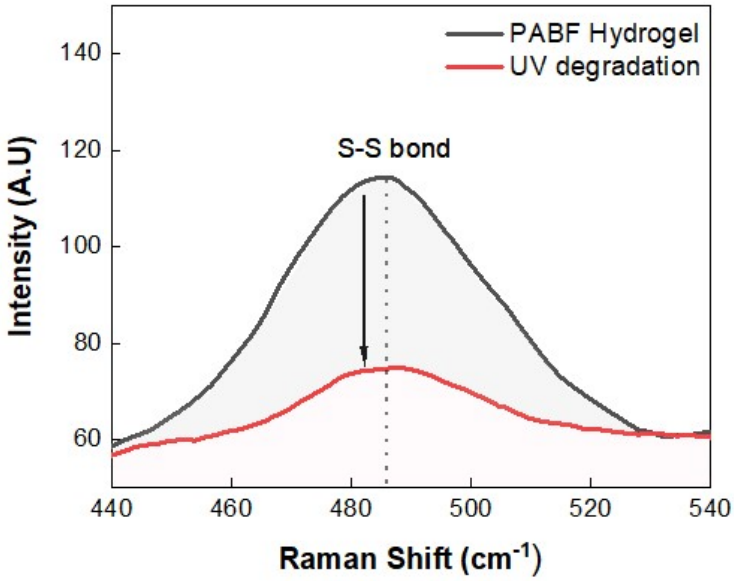

Figure S2. Raman spectral analysis of the PABF hydrogel before and after UV irradiation, showing a decrease in the characteristic disulfide (S–S) stretching band due to UV-induced cleavage of disulfide bonds.

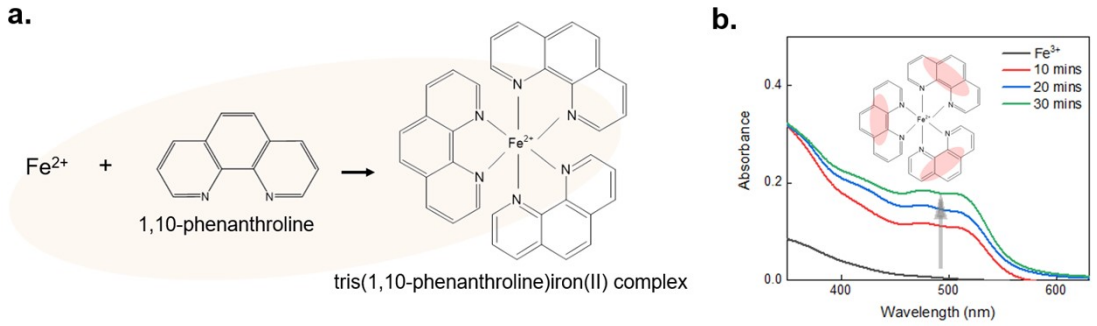

Figure S3. UV–Vis verification of UV-induced photoreduction of Fe^{3+} to Fe^{2+}. (a) Schematic illustration of the formation of the Fe^{2+}–1,10-phenanthroline complex used for Fe^{2+} detection. (b) UV–Vis absorption spectra showing the gradual increase of the characteristic absorption peak near ~510 nm with increasing UV irradiation time, confirming time-dependent photoreduction of Fe^{3+}.

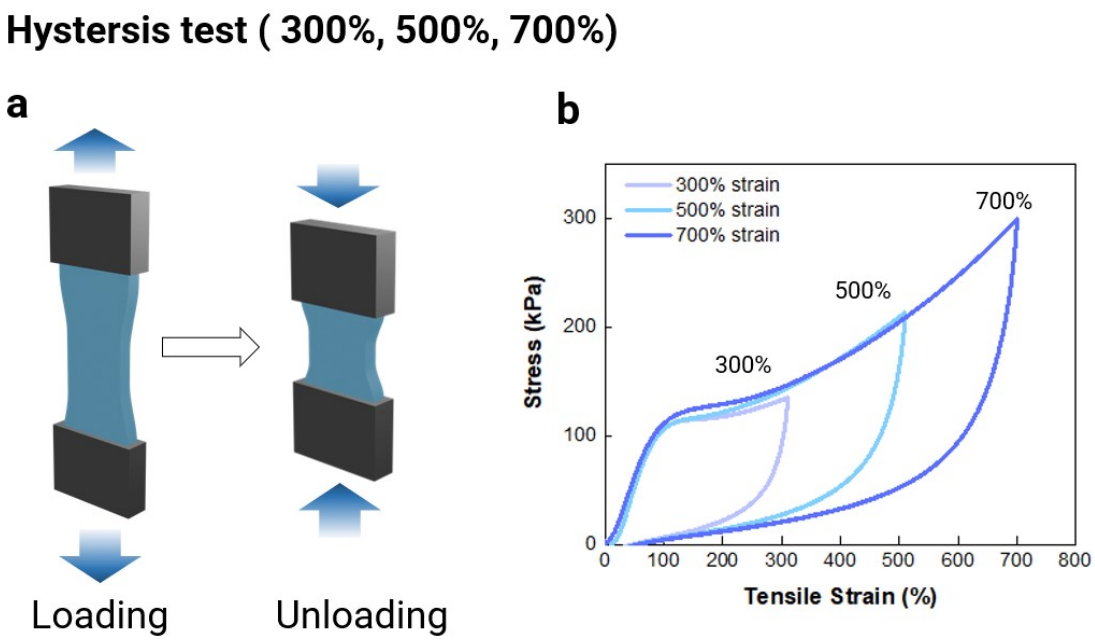

Figure S4. Hysteresis test of the PABF hydrogel, showing (a) a schematic illustration of the hysteresis test setup and (b) tensile stress–strain hysteresis curves of the hydrogel at 300%, 500%, and 700% strain. Data represent a single measurement.

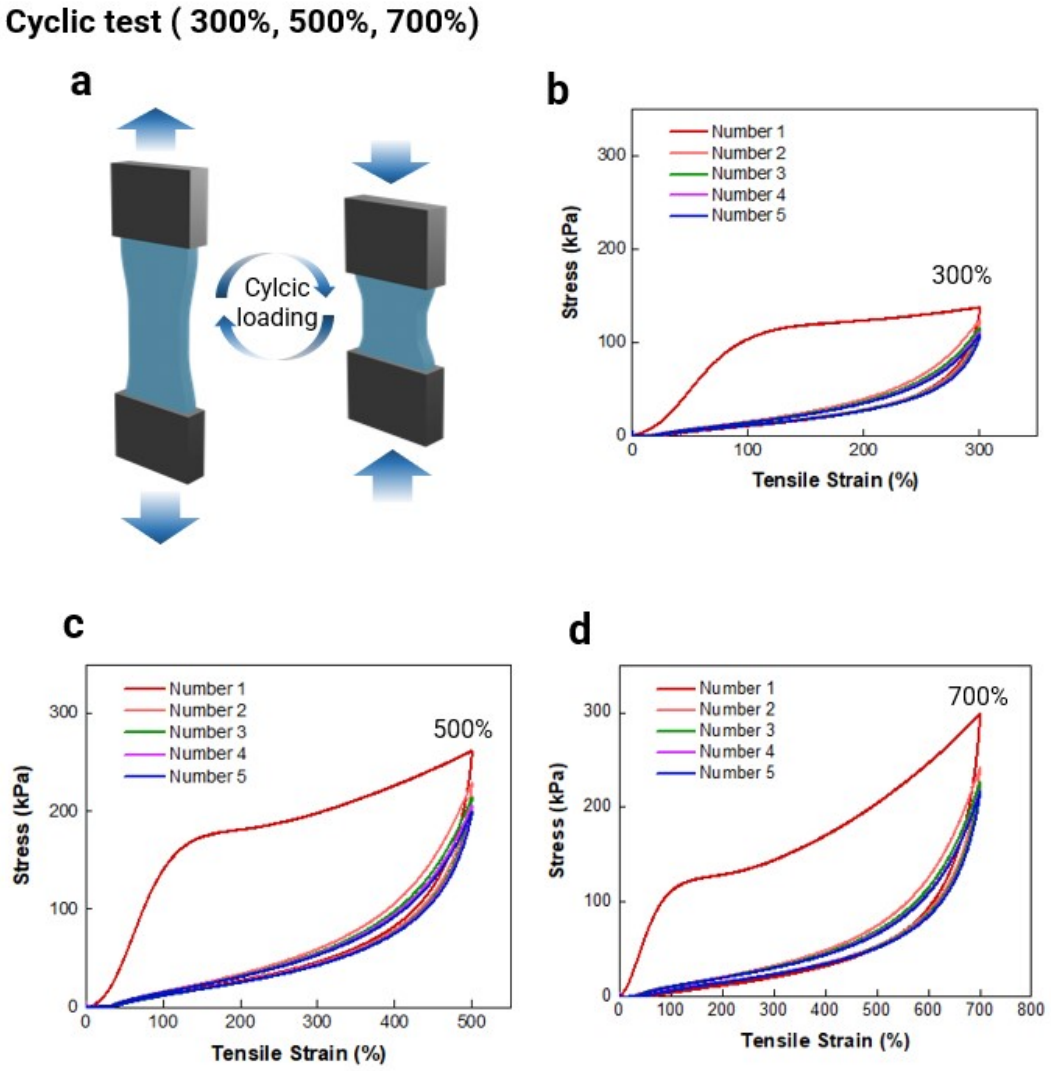

Figure S5. Cyclic tensile test of the PABF hydrogel, showing (a) a schematic illustration of the cyclic test setup and (b–d) stress–strain curves of the hydrogel under cyclic loading at 300%, 500%, and 700% strain, respectively. Data represent a single measurement.

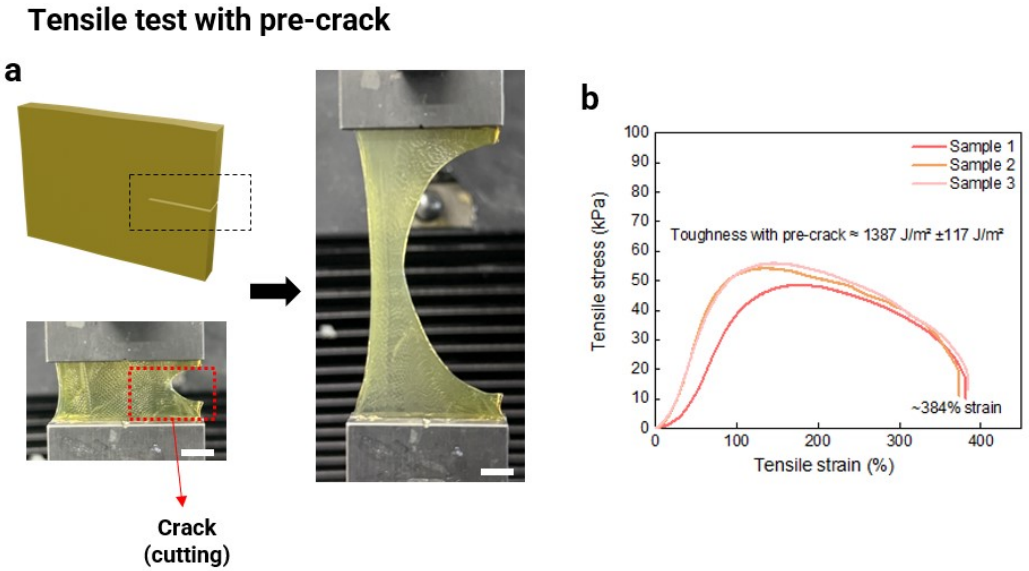

Figure S6. Tensile test of the PABF hydrogel with a pre-crack, showing (a) a schematic illustration and photographs of the pre-cracked sample during tensile testing, and (b) the corresponding stress–strain curve of the pre-cracked hydrogel sample. Data represent a single measurement. Scale bars, 5mm.

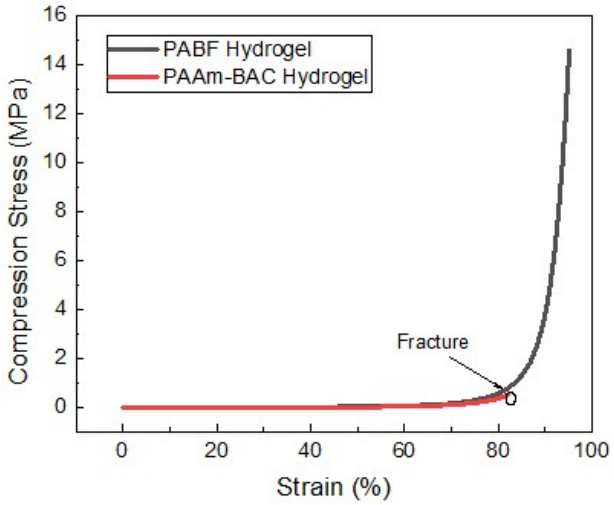

Figure S7. Compression test of the PABF hydrogel. Stress–strain curves obtained from compressive loading of the PABF hydrogel compared with a single-network PAAm–BAC hydrogel used as a control.

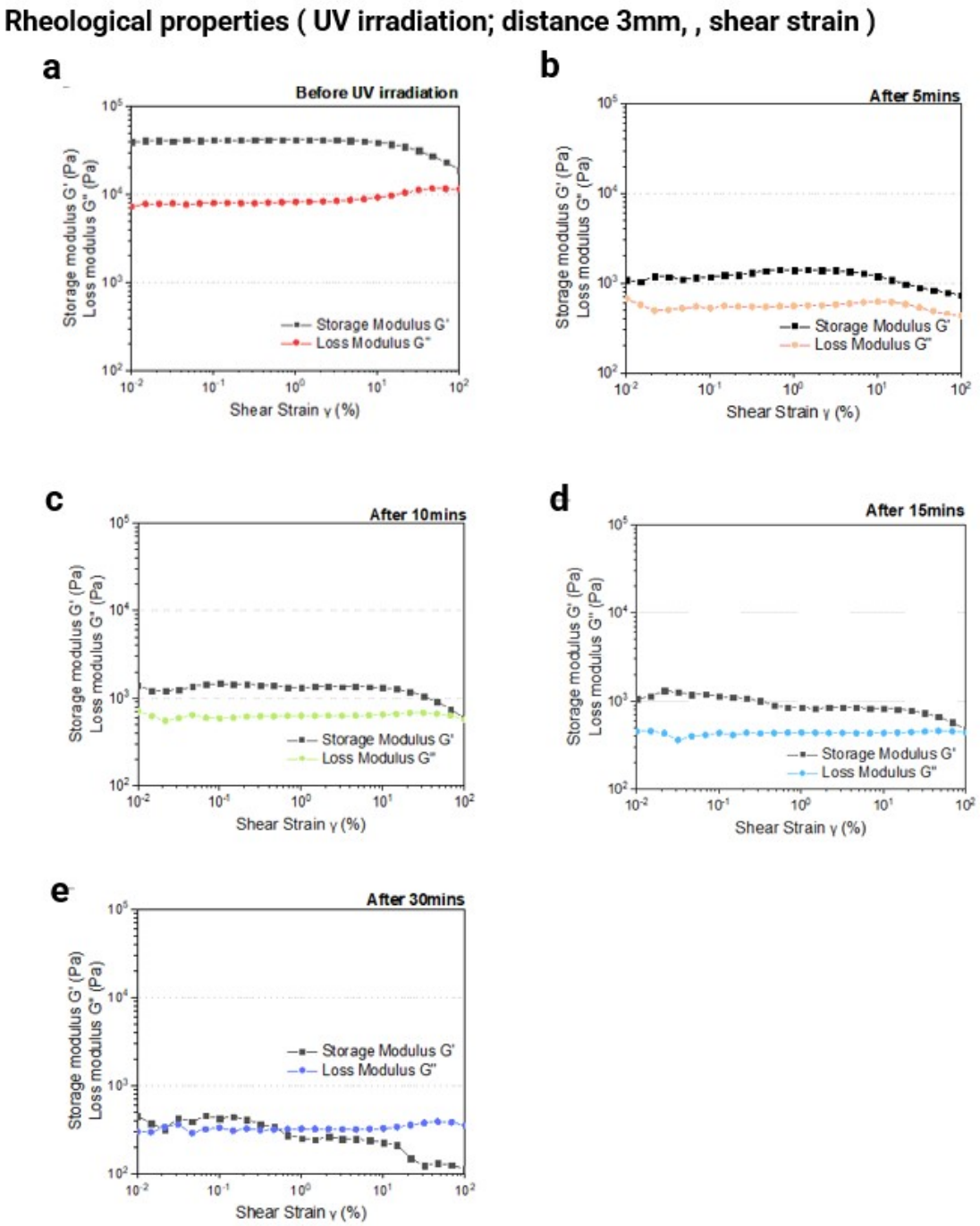

Figure S8. Rheological analysis of the PABF hydrogel under UV irradiation in amplitude sweep mode. (a) before irradiation, (b) after 5 min, (c) after 10 min, (d) after 15 min, and (e) after 30 min of UV exposure. Data represent a single measurement.

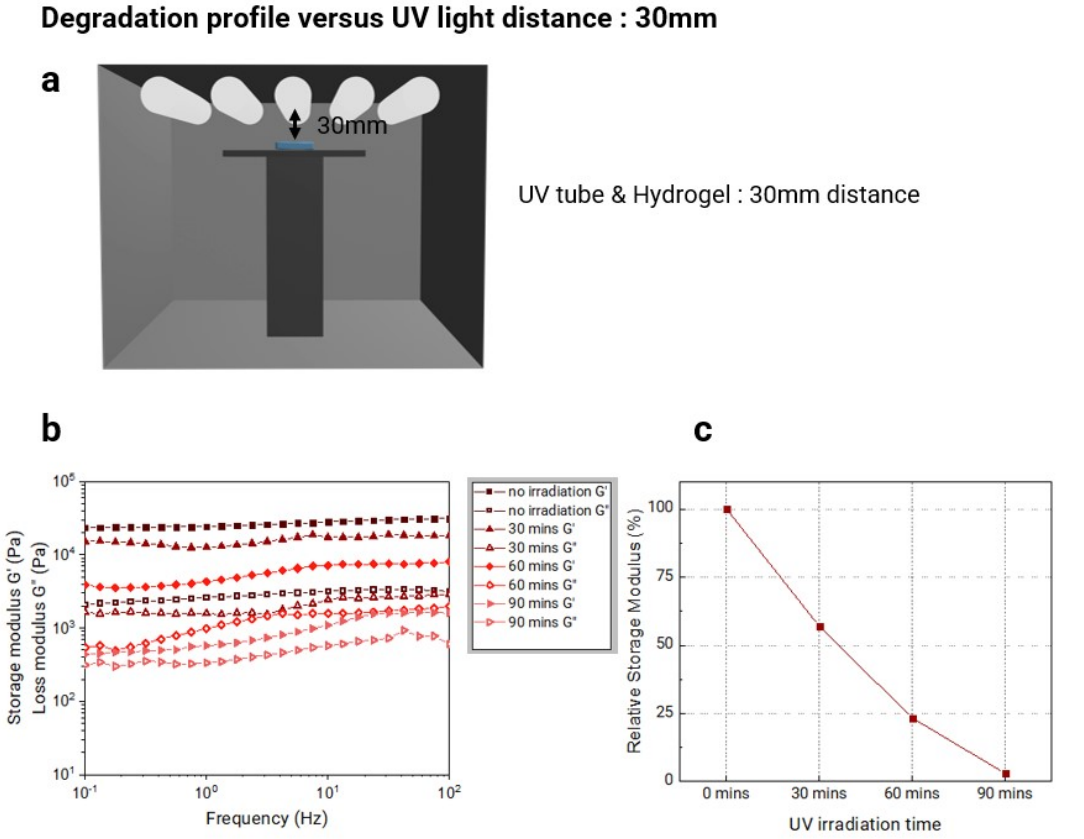

Figure S9. Rheological analysis of the PABF hydrogel degradation profile under UV irradiation with a lamp-to-sample distance of 30 mm. (a) schematic illustration of the experimental setup, (b) rheological measurements showing changes during UV exposure, and (c) relative decrease in storage modulus as a function of irradiation time. Data represent a single measurement.

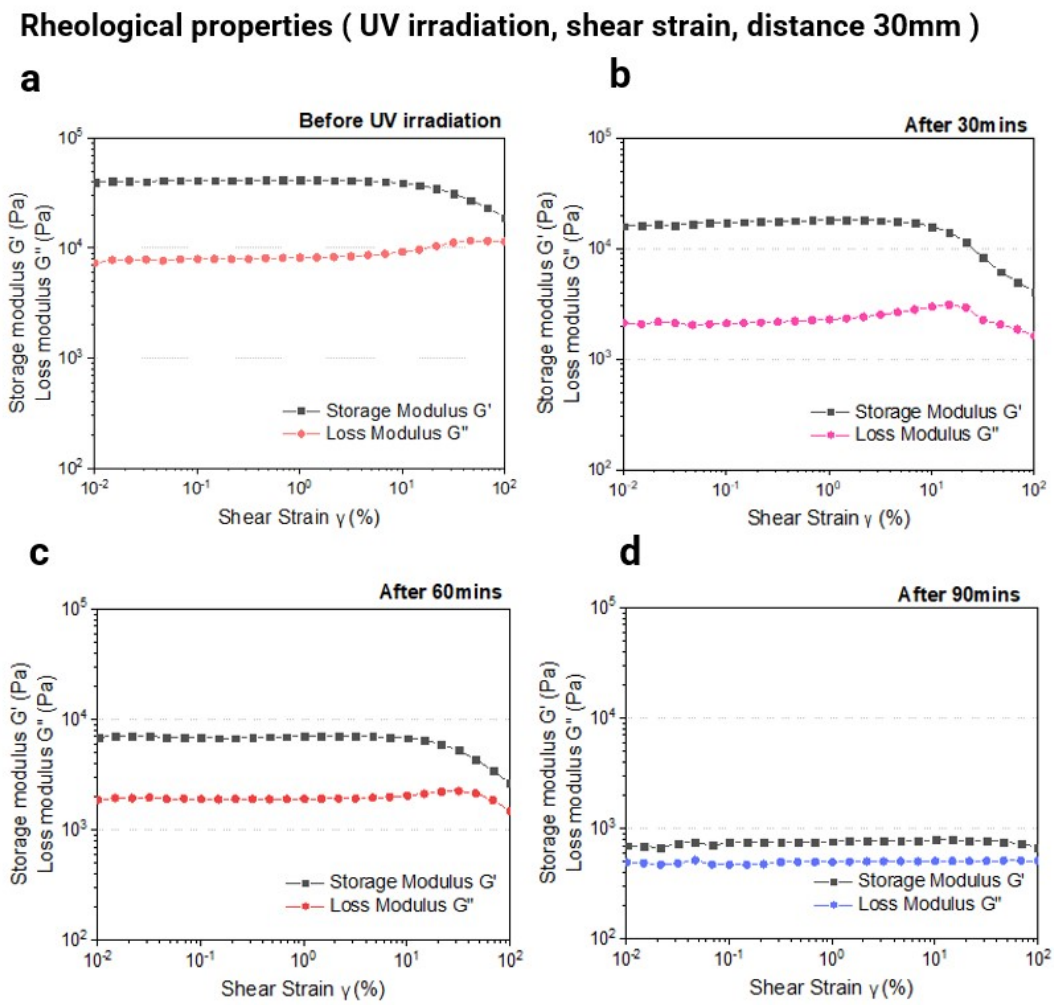

Figure S10. Rheological analysis of the PABF hydrogel in amplitude sweep mode under UV irradiation with a lamp-to-sample distance of 30 mm. (a) before irradiation, (b) after 30 min, (c) after 60 min, and (d) after 90 min of UV exposure. Data represent a single measurement.

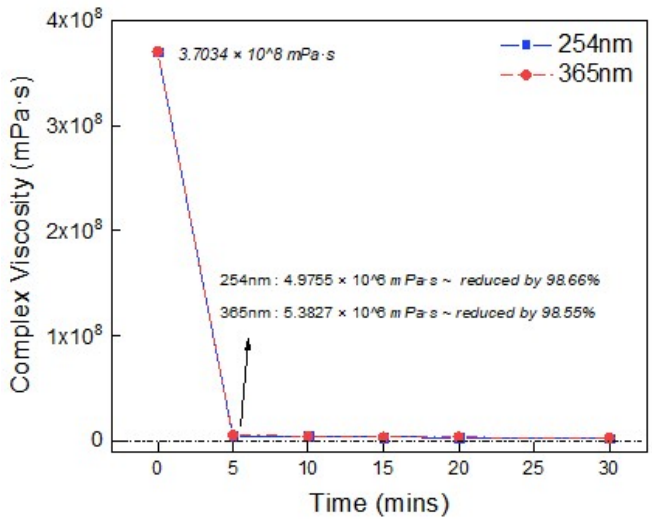

Figure S11. Comparison of complex viscosity changes of the PABF hydrogel under 254 nm and 365 nm UV irradiation as a function of irradiation time.

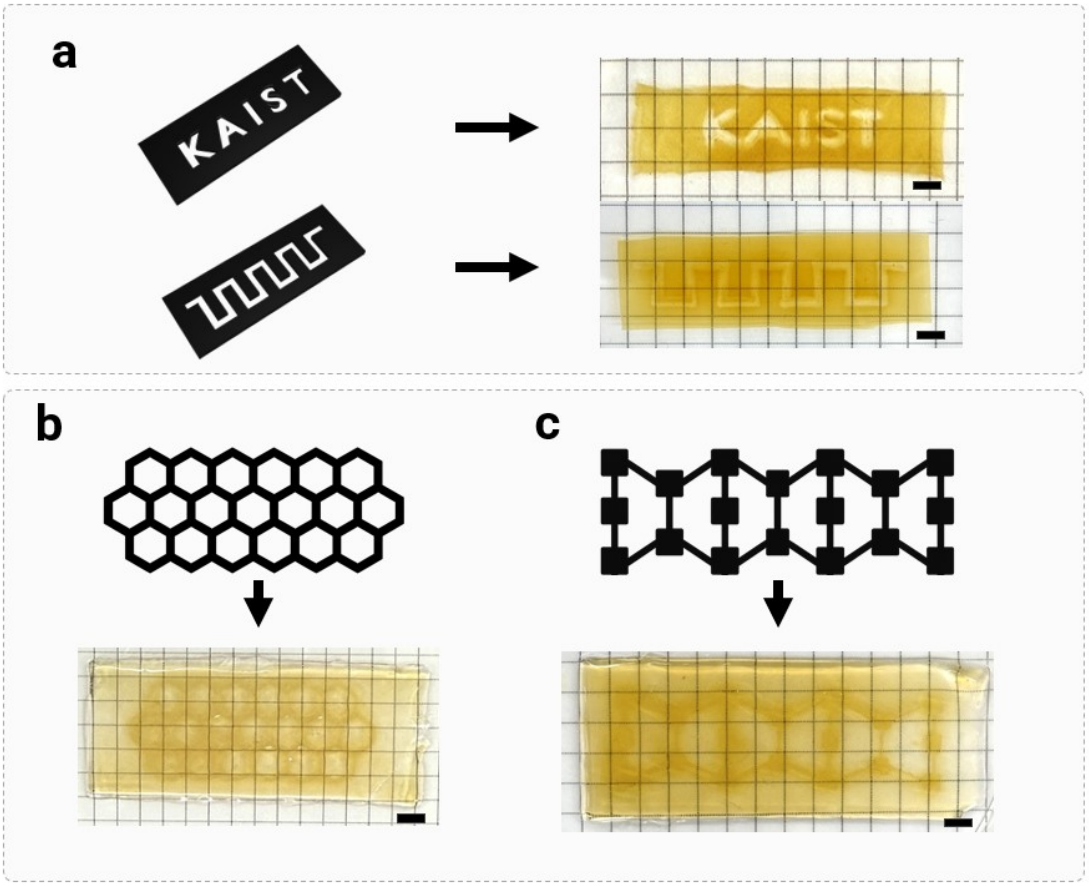

Figure S12. Formation of various patterns using the PABF hydrogel. (a) Photopatterning of the hydrogel into lettering ("KAIST") and line shapes using designed photomasks. (b) Fabrication of complex structures such as honeycomb patterns. (c) Intricate geometric patterns. Pattern dimensions are indicated in the images. The photomasks were fabricated by laser cutting with a practical resolution of approximately ~1 mm. Scale bars, 5 mm.

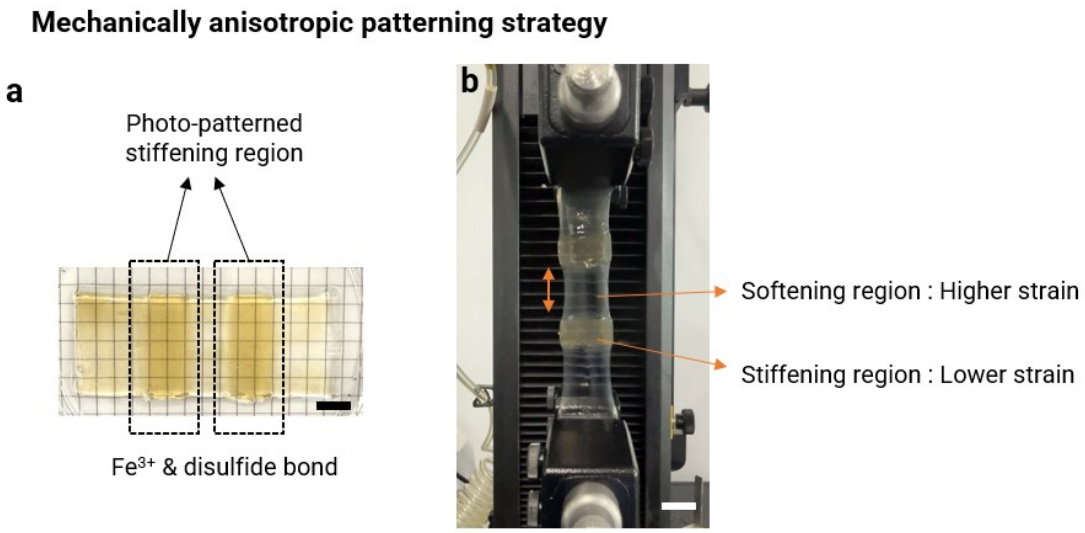

Figure S13. Mechanically anisotropic patterning strategy of the PABF hydrogel. (a) photograph showing selective UV irradiation to create patterned stiffened regions within the hydrogel. (b) tensile testing image of the patterned hydrogel, where the transparent (non-irradiated) regions exhibit higher strain compared to the irradiated areas. Scale bars, 10mm.

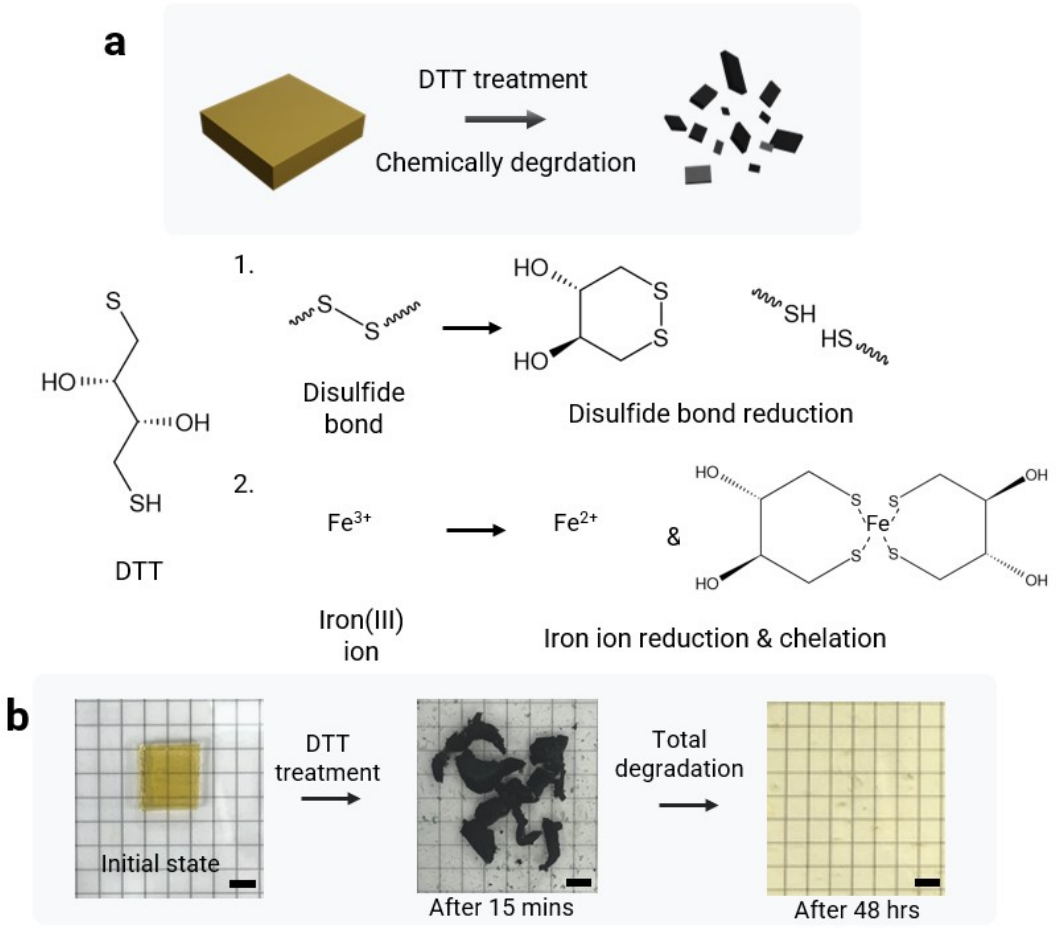

Figure S14. Chemical degradation of the PABF hydrogel induced by DTT treatment. (a) schematic illustration showing the reaction of DTT with the hydrogel crosslinkers. (b) photographic images demonstrating the progressive degradation of the PABF hydrogel during DTT treatment. Scale bars, 5mm.

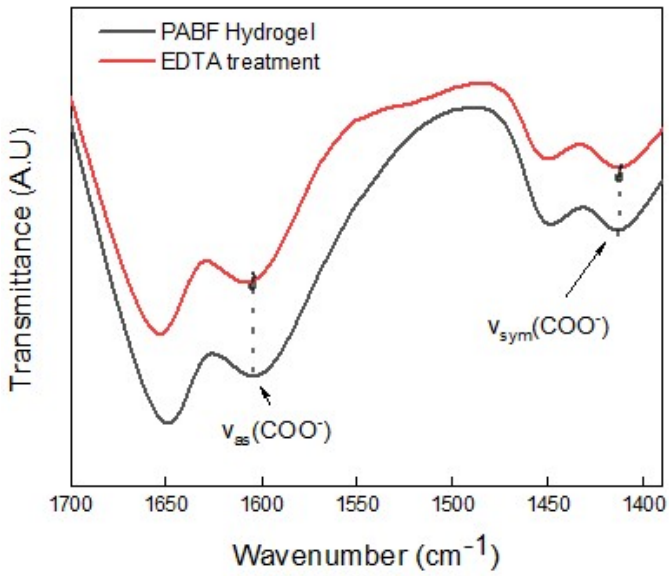

Figure S15. FT-IR spectra of the PABF hydrogel before and after EDTA treatment, showing changes in the carboxylate-related bands at ~1600 cm^{-1} (ν_as(COO^-)) and ~1400 cm^{-1} (ν_sym(COO^-)).

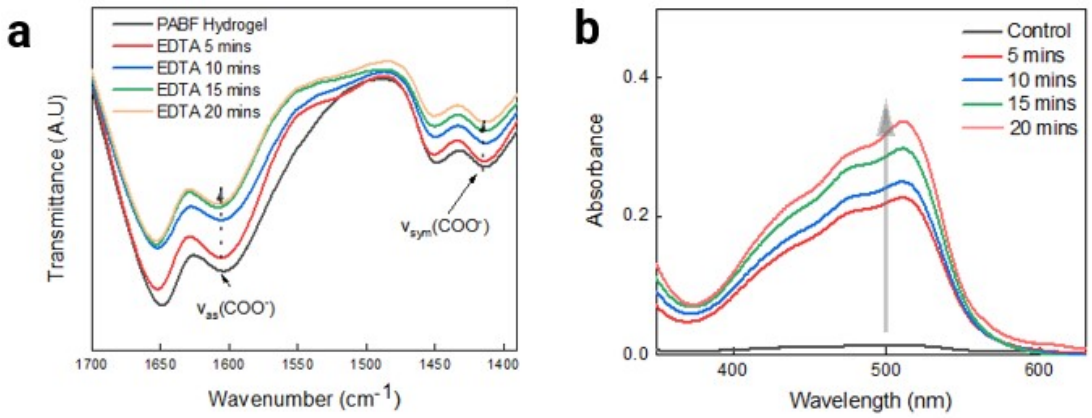

Figure S16. Time-dependent analysis of Fe^{3+} removal during EDTA treatment. (a) FT-IR spectra of the PABF hydrogel after 5–20 min EDTA treatment. (b) UV–Vis spectra of Fe^{2+}–phenanthroline complexes formed from Fe ions released during EDTA treatment, showing increasing absorbance at ~510 nm with time.

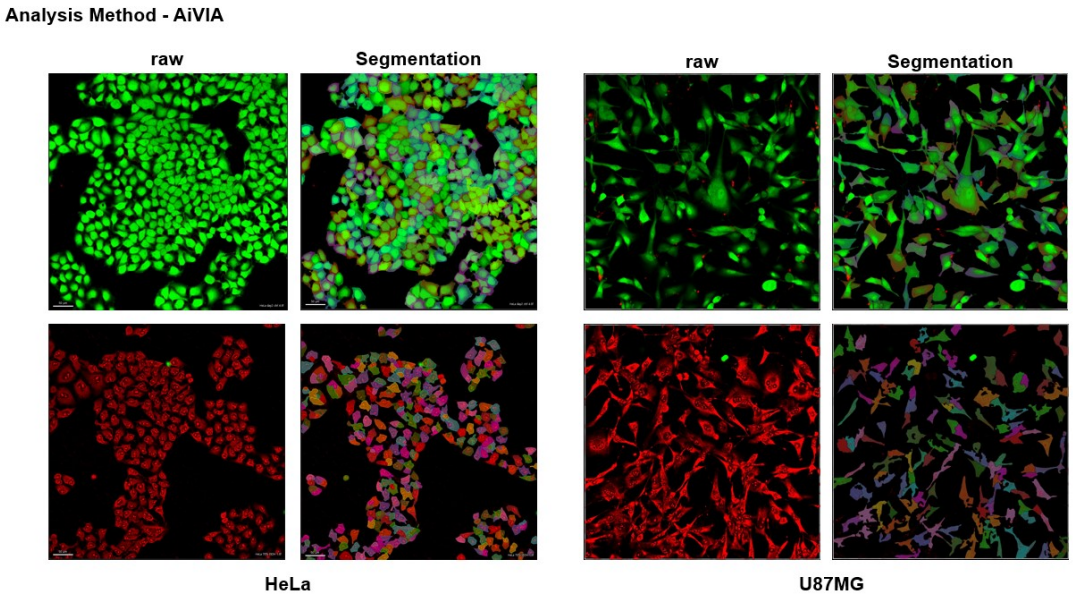

Figure S17. AI-based cell segmentation of LIVE/DEAD images using Aivia software. Raw images and corresponding segmentation outputs for HeLa and U87MG cells used for automated counting of live (488 nm) and dead (546 nm) cells.

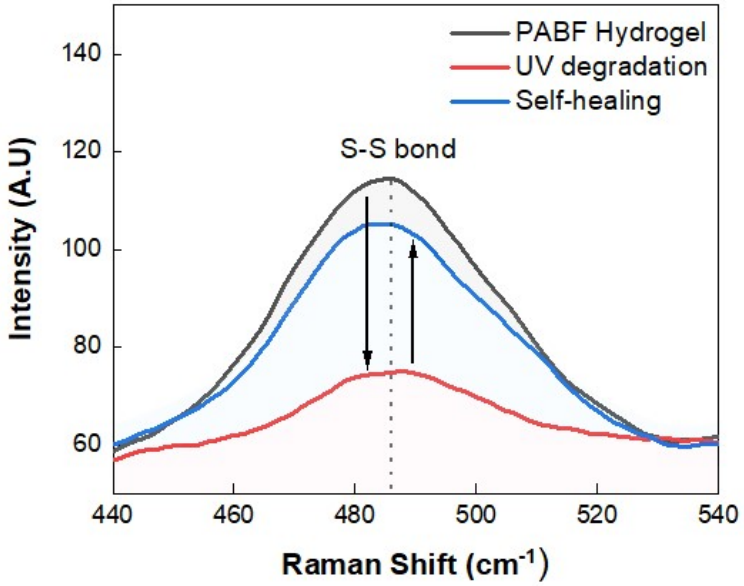

Figure S18. Raman spectra of the PABF hydrogel showing changes in the disulfide (S–S) stretching band before UV irradiation, after UV degradation, and after self-healing.

.

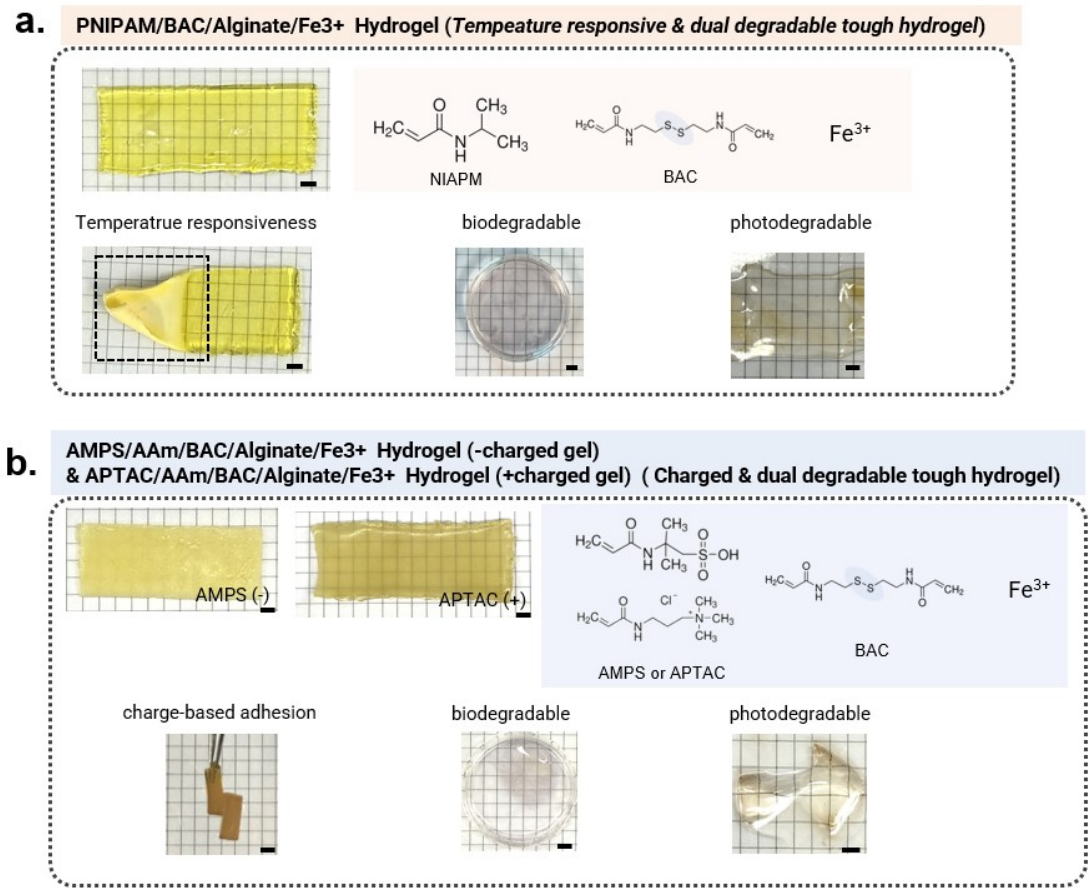

Figure S19. Generalization of the BAC + Fe^{3+} crosslinking strategy for dual-degradable hydrogels. Various functional monomers were incorporated to demonstrate the versatility of the system. (a) Fabrication of a dual-degradable hydrogel using the thermoresponsive monomer NIPAM. (b) Fabrication of dual-degradable hydrogels using charged monomers AMPS and APTAC.